Shaped graded materials with an apparent negative thermal conductivity

C. Z. Fan, Y. Gao, and J. P. Huang[a)]
Surface Physics Laboratory (National Key Laboratory) and Department of Physics, Fudan University, Shanghai 200433, People's Republic of China

(Received 11 February 2008; accepted 5 June 2008; published online 24 June 2008)

Based on a first-principles approach, we exploit a class of shaped graded materials in which thermal energy is apparently controlled to transfer from a region of lower temperature to a region of higher temperature. This phenomenon, which is in contrast to our common intuition, is indicative of an apparent negative thermal conductivity (ANTC). Further analysis shows that the ANTC is related to a symmetric oscillation of paired thermal conductivities with specific gradation profiles, which are shown to satisfy a sum rule. Such shaped graded materials can serve as good candidates for thermal rectification. © *2008 American Institute of Physics*. [DOI: 10.1063/1.2951600]

First we briefly review the recent development of various cloaks,[1–10] which were designed by using graded materials.[11] An electromagnetic cloak is well known for hiding objects from electromagnetic waves,[1–3] due to the high freedom of design of metamaterials[12] that may be both inhomogeneous and anisotropic in their electric permittivity and magnetic permeability. Independently, Leonhardt[4,5] has given an approach that can be performed to cloak an object in the short wavelength limit. Owing to intriguing potential applications related to such invisibility, such an electromagnetic cloak has received extensive attention, e.g., ranging from its scattering cross section[6] and two dimensional counterpart,[2,7–9] to its extensions such as acoustic cloaks.[10] In this work, we initially start by proposing a kind of thermal cloaks. Interestingly, based on a coordinate transformation method, we exactly reveal an inverse thermal flow (ITF) as geometric shape of the cloak changes in a typical range. The ITF is indicative of an apparent negative thermal conductivity (ANTC). The ANTC is of value for achieving various thermal rectifications, e.g., designing thermal diodes.[13–16] They have potential important applications such as environmentally friendly air conditions. To realize them, the present mechanism is distinctly different from that used in Refs. 13 and 14.

Thermal conduction is the movement of a heat flux from a high temperature region toward a low temperature region. In this process, the heat flux is proportional to the temperature gradient. The thermal conduction equation can be written as

$$\rho C\frac{\partial T}{\partial t}+\nabla(-\kappa\nabla T)=Q, \tag{1}$$

where ρ is the density, C is the heat capacity, T is the temperature, κ is the thermal conductivity, and Q is a heat source. For a steady state, temperature T does not change with time thus the first term containing $\partial T/\partial t$ vanishes. Throughout this work, there is no heat source in the area under consideration, so $Q=0$. Thus, Eq. (1) admits $\nabla(-\kappa\nabla T)=0$.

In the Cartesian coordinates (x,y,z), the equation for describing an ellipsoidal shape is $x^2/a^2+y^2/b^2+z^2/c^2=1$, where a, b, and c are the three principal semiaxes of the ellipsoid. We choose (λ,μ,ν) to represent a point in the ellipsoidal coordinates. Then, we squeeze the ellipsoidal volume into an ellipsoidal shell through the following relations $\lambda'=a_1+\lambda(a_2-a_1)/a_2$, $\mu'=b_1+\mu(b_2-b_1)/b_2$, and $\nu'=c_1+\nu(c_2-c_1)/c_2$, where a_1, b_1, and c_1 (a_2, b_2, and c_2) are the inner (outer) three principal semiaxes of the ellipsoidal shell. The key feature of the permittivity equations which allows the invisibility is the invariance of their form under coordinate transformations.[1,17] In the present distorted coordinates, the form of the thermal conduction equation also keeps unchanged, but the corresponding thermal conductivity is got in the form like $\kappa'_{\lambda'}=\kappa_\lambda Q_\lambda Q_\mu Q_\nu/Q_\lambda^2$, where κ_λ is thermal conductivity in the original coordinates, and Q_λ, Q_μ, and Q_ν are[2]

$$Q_\lambda=\left(\frac{\partial x}{\partial\lambda}\right)^2+\left(\frac{\partial y}{\partial\lambda}\right)^2+\left(\frac{\partial z}{\partial\lambda}\right)^2, \tag{2}$$

$$Q_\mu=\left(\frac{\partial x}{\partial\mu}\right)^2+\left(\frac{\partial y}{\partial\mu}\right)^2+\left(\frac{\partial z}{\partial\mu}\right)^2, \tag{3}$$

$$Q_\nu=\left(\frac{\partial x}{\partial\nu}\right)^2+\left(\frac{\partial y}{\partial\nu}\right)^2+\left(\frac{\partial z}{\partial\nu}\right)^2. \tag{4}$$

Thus, in the distorted ellipsoidal coordinates, we have the renormalized values of the thermal conductivities, $\kappa'_{\lambda'}$, $\kappa'_{\mu'}$, and $\kappa'_{\nu'}$, inside the ellisoidal cloaking region (shell),

$$\kappa'_{\lambda'}=\frac{a_2}{a_2-a_1}\frac{b_2}{b_2-b_1}\frac{c_2}{c_2-c_1}\frac{(\lambda'-a_1)^2}{\lambda'^2}\kappa_0, \tag{5}$$

$$\kappa'_{\mu'}=\frac{a_2}{a_2-a_1}\frac{b_2}{b_2-b_1}\frac{c_2}{c_2-c_1}\frac{(\mu'-b_1)^2}{\mu'^2}\kappa_0, \tag{6}$$

$$\kappa'_{\nu'}=\frac{a_2}{a_2-a_1}\frac{b_2}{b_2-b_1}\frac{c_2}{c_2-c_1}\frac{(\nu'-c_1)^2}{\nu'^2}\kappa_0, \tag{7}$$

where κ_0 denotes the thermal conductivity of the host material (which is beyond the whole cloak). From Eqs. (5)–(7), we can see that the thermal conductivity κ' is both anisotropic and tensorial (see also Fig. 1).

Now we are in a position to perform numerical simulations by using the finite element method. There are three domains in the whole system, namely, the inner domain, the cloaking domain (shell), and the outer domain. For convenience, we set the thermal conductivity of the inner domain to have the same value as that κ_0 of the outer domain, and

a)Electronic mail: jphuang@fudan.edu.cn.

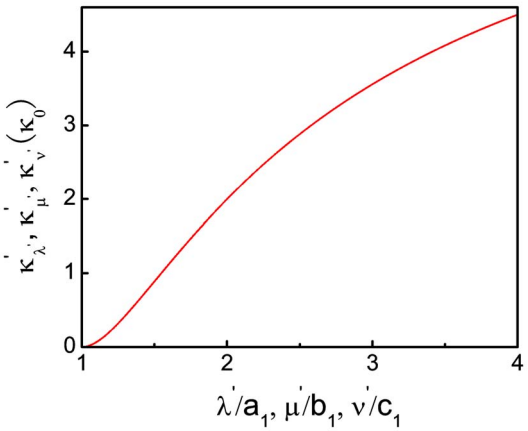

FIG. 1. (Color online) The anisotropic thermal conductivities $\kappa'_{\lambda'}$, $\kappa'_{\mu'}$, and $\kappa'_{\nu'}$ in the distorted coordinate vs λ'/a_1, μ'/b_1, and ν'/c_1, respectively, according to Eqs. (5)–(7). The three curves are overlapped. Parameters: $a_2=2a_1$, $b_2=2b_1$, and $c_2=2c_1$.

$\kappa_0=163$ W/m K (thermal conductivity of silicon). This will not affect our results at all because the main interest of this work is on the cloaking domain, in which the behavior of ITF appears. The thermal conductivity of the cloaking domain is determined according to Eqs. (5)–(7). For all the spherical or non-spherical cloaks discussed in this work, we keep the ratio between the volume of the cloaking (shell) domain and that of the inner domain to be 7:1, and the applied temperature T is set to be 300 and 100 K at the two opposite planes of the cubic simulation box, respectively. It is worth mentioning that, regardless of the actual value of T, our results hold for given temperature differences between the opposite planes. As the spherical cloak is centrosymmetric, it makes no difference when the temperature is applied in various directions. However, for an ellipsoidal cloak, we have to discriminate the direction of temperature due to the existence of geometric anisotropy. In our simulations, we apply the temperature in two opposite planes along the three principal axes, a, b, and c, of the ellipsoidal cloak, respectively. Below we focus on two types of rotational ellipsoid (namely, spheroid) with $a<b=c$ (oblate spheroid) and $a>b=c$ (prolate spheroid). Throughout this work, the set of a,b, and c will be used to denote both three inner semiaxes (a_1, b_1, and c_1) and three outer semiaxes (a_2, b_2, and c_2) of the ellipsoidal cloak if there are no special instructions. We should remark that our simulation results are also independent of the length scale of the cloak, e.g., from microsized to macrosized, if any.

Figure 1 displays the anisotropic thermal conductivities $\kappa'_{\lambda'}$, $\kappa'_{\mu'}$, and $\kappa'_{\nu'}$ in the distorted coordinate versus λ'/a_1, μ'/b_1, and ν'/c_1, respectively, according to Eqs. (5)–(7). A monotonic increase is clearly shown.

Figure 2 shows the pathway of heat flux in thermal cloaks with various geometrical shapes. The temperature distribution is also shown. The streamlines of Fig. 2(a) represent the pathway of the heat flux in the spherical cloak for the parameters as indicated in the caption. As we can see, the heat flux goes around the inner domain and eventually returns to its original pathway. In this process, the object inside the inner domain is protected from the invasion of external heat flux. For a spheroidal cloak, the pathway of the heat flux is also illustrated in Fig. 2(b) (oblate spheroid) and Fig. 2(c) (prolate spheroid) with the applied temperature gradient directed along the principal semiaxis a. The pathway of the oblate spheroidal cloak with $a<b=c$ is similar to that of the

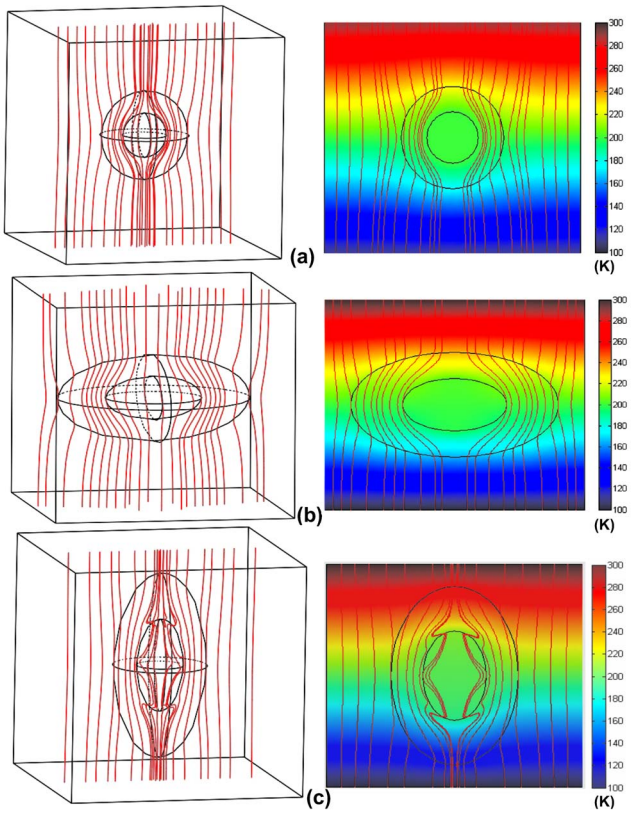

FIG. 2. (Color online) Pathway of heat flux in thermal cloaks (left panels) and their cross sections (right panels). The streamlines denote the pathway of the heat flux when the temperature is set to be 300 and 100 K at the top and bottom planes of the cubic simulation box, respectively. The temperature distribution is also shown in the cross section. (a) Spherical thermal cloak and its cross section. Parameters: $r_1=0.1$ m (inner radius) and $r_2=0.2$ m (outer radius). (b) Oblate spheroidal thermal cloak with three principal semiaxes a, b, and c satisfying $a<b=c$ (left panel) and its cross section (right panel). The temperature gradient is applied along the direction of the semi-axis a. Parameters: $a_1=0.1$ m and $b_1=c_1=0.2$ m (three inner semiaxes); $a_2=0.2$ m and $b_2=c_2=0.4$ m (three outer semiaxes). (c) Same as (b), but for prolate spheroidal thermal cloak with $a>b=c$. Parameters: $a_1=0.2$ m and $b_1=c_1=0.1$ m; $a_2=0.4$ m and $b_2=c_2=0.2$ m.

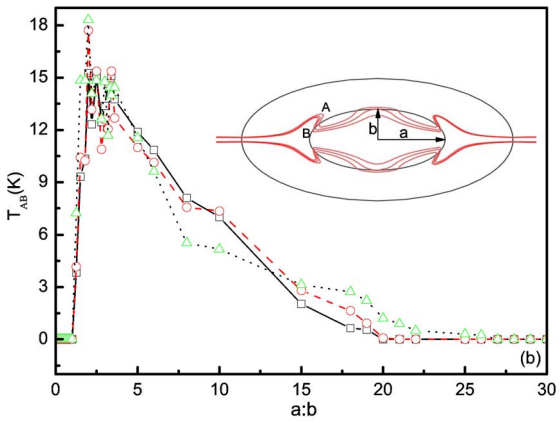

FIG. 3. (Color online) Temperature difference T_{AB} between the starting point A and ending point B of the ITF streamline (as indicated in the inset) as a function of the ratio between a and b ($a:b$) for spheroidal thermal cloaks with three principal semiaxes $a\neq b=c$. The three curves correspond to three positions of incoming heat flux that respectively, have vertical distances of $0.8b$, $0.6b$, and $0.4b$ with respect to the semiaxis a (see also the inset).

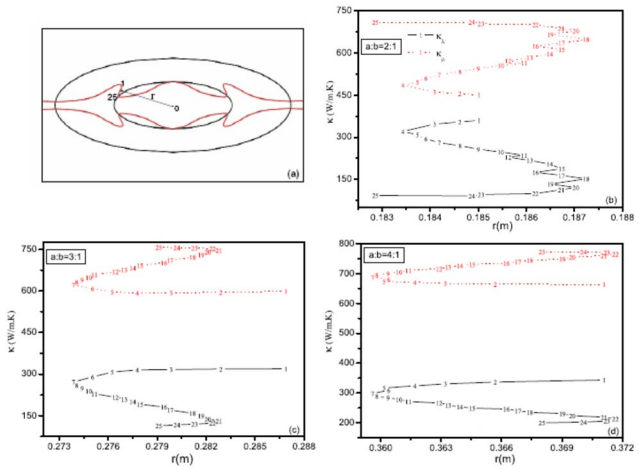

FIG. 4. (Color online) Paired thermal conductivities $\kappa'_{\lambda'}$ and $\kappa'_{\mu'}$ (indicated by the same number) in the ITF streamlines within the cross section of the prolate spheroidal cloak with $a>b=c$ as a function of the distance r between any point in the ITF streamline and the center of the cloak [see (a) the schematic graph], for (b) $a:b=2:1$, (c) $a:b=3:1$, and (d) $a:b=4:1$. All the 25 points have been taken in sequence from the starting point to the ending point of the ITF streamlines, as clearly indicated in the corresponding ordered numbers [see (a)].

spherical cloak. However, the situation becomes different for the case of prolate spheroid with $a>b=c$, as shown in Fig. 2(c). We observe an ITF inside the prolate spheroidal cloak. Here, the so-called ITF means that the heat flux can flow backwards, in contrast to normal thermal flow (NTF) for which the heat flux flows forward only. The ITF corresponds to an ANTC in this nonspherical cloaking region, which is to be explained below. Due to the symmetry of the prolate spheroid, the ITF zone is strictly symmetrical, which locates close to the two opposite sides of the prolate cloak. Furthermore, we have also investigated the case of a general ellipsoid with $a\neq b\neq c$ for which the external temperature gradient is directed along the longest principal semiaxis, and its behavior is generally similar to Fig. 1(c) (no figures shown here). Nevertheless, in this case, the ITF streamline is no longer strictly symmetrical, the degree of which depends on the actual values of a, b, and c.

For understanding the ITF, we resort to the Fourier thermal conduction equation,[18]

$$J_T = -\kappa\frac{dT}{dz} = -\kappa\frac{\Delta T}{\Delta z}, \tag{8}$$

where J_T is heat flux density, κ is the thermal conductivity, and ΔT is the temperature gradient. This equation indicates that the thermal flux should flow from the high temperature region to the low temperature region. So, as for homogeneous materials (or without the thermal cloak of our interest), the temperature difference between positions A and B (see Fig. 3), T_{AB}, should be smaller than zero, namely, $T_A<T_B$. That is, in this situation, the thermal flux should flow from B to A. However, in the present case (with the thermal cloak), the local temperature difference between the two points A and B T_{AB} is larger than zero indeed as to be shown in Figs. 3 and 4, namely, $T_A>T_B$. Moreover, the thermal flux still flows from point A to B. This is apparently opposite to the requirement of the homogeneous case. Thus, this corresponds to an ANTC in the inverse region, which arises from the specific profile of material properties.

In Fig. 3, we discuss the temperature gradient along the direction of the semiaxis a. Here, the temperature difference T_{AB} (see the caption) is investigated as a function of the ratio between a and b $(a:b)$. In detail, there is a coexistence of NTF and ITF streamlines, and a transition between them as geometrical shape of the cloak varies. Evidently, when $a:b$ is smaller than or equal to 1 (oblate spheroid or sphere), the temperature difference $T_{AB}=0$, namely, there is no ITF, and only NTF appears. As $a:b>1$ (prolate spheroid), the ITF comes to appear, and reaches maximum at about $a:b=2$. Eventually, it tends to disappear as $a:b$ is large enough corresponding to a rodlike cloak.

Figure 4 displays the relation between the thermal conductivities $\kappa'_{\lambda'}$ and $\kappa'_{\mu'}$ in the ITF region within the cross section of the spheroidal cloaking domain as a function of the distance r (details can be found in the caption). All the 1–25 points displayed in (b)–(d) have been taken in sequence along the streamline of the ITF region, as shown in Fig. 4(a), which are indicated by the ordered numbers for $a:b=$ (b) 2:1, (c) 3:1, and (d) 4:1. As $a:b$ is given, all the paired $\kappa'_{\lambda'}$ and $\kappa'_{\mu'}$ (namely, two thermal conductivities corresponding to the same number) appear in a symmetric oscillation trajectory, and satisfy a sum rule: $\kappa'_{\lambda'}+\kappa'_{\mu'}=$(b) 802.7 ± 0.6, (c) 889 ± 3, and (d) 984 ± 2. It is worth noting that the corresponding thermal conductivity $\kappa'_{\nu'}$ keeps unchanged for the cross section (in two dimensions) of interest.

The fact that our results do not depend on specific length scales makes an experimental demonstration very tractable. Finally, it should be noted that, besides thermal conduction of our interest, heat can also be transferred by thermal radiation and/or convection, and that often more than one of these processes occur in a particular situation.

This work was supported by the Pujiang Talent Project (No. 06PJ14006) of the Shanghai Science and Technology Committee, by the Shanghai Education Committee (Shuguang project), by the NSFC under Grant No. 10604014, and by CNKBRSF under Grant No. 2006CB921706.

[1] J. B. Pendry, D. Schurig, and D. R. Smith, Science **312**, 1780 (2006).
[2] D. Schurig, J. B. Pendry, and D. R. Smith, Opt. Express **14**, 9794 (2006).
[3] D. Schurig, J. J. Mock, B. J. Justice, S. A. Cummer, J. B. Pendry, A. F. Starr, and D. R. Smith, Science **314**, 977 (2006).
[4] U. Leonhardt, Science **312**, 1777 (2006).
[5] U. Leonhardt, New J. Phys. **8**, 118 (2006).
[6] H. Chen, B. Wu, B. Zhang, and J. A. Kong, Phys. Rev. Lett. **99**, 063903 (2007).
[7] W. Cai, U. K. Chettiar, A. V. Kildishev, and V. M. Shalaev, Nat. Photonics **1**, 224 (2007).
[8] Z. Ruan, M. Yan, C. W. Neff, and M. Qiu, Phys. Rev. Lett. **99**, 113903 (2007).
[9] M. Yan, Z. Ruan, and M. Qiu, Phys. Rev. Lett. **99**, 233901 (2007).
[10] H. Y. Chen and C. T. Chan, Appl. Phys. Lett. **91**, 183518 (2007).
[11] For example, see J. P. Huang and K. W. Yu, Phys. Rep. **431**, 87 (2006); Appl. Phys. Lett. **85**, 94 (2004).
[12] D. R. Smith, J. B. Pendry, and M. C. K. Wiltshire, Science **305**, 788 (2004).
[13] B. Li, L. Wang, and G. Casati, Phys. Rev. Lett. **93**, 184301 (2004).
[14] C. W. Chang, D. Okawa, A. Majumdar, and A. Zettl, Science **314**, 1121 (2006).
[15] N. Yang, N. Li, L. Wang, and B. Li, Phys. Rev. B **76**, 020301(R) (2007).
[16] G. Wu and B. Li, Phys. Rev. B **76**, 085424 (2007).
[17] G. W. Milton, M. Briane, and J. R. Willis, New J. Phys. **8**, 248 (2006).
[18] J. M. Ziman, *Principles of the Theory of Solids*, 2nd ed. (Cambridge University Press, England, 1972).